Generation of Gigawatt Circularly Polarized Attosecond-Pulse Pairs

K. Hu[1] and H.-C. Wu[1,2,*]
[1]Institute for Fusion Theory and Simulation and Department of Physics, Zhejiang University, Hangzhou 310027, China
[2]IFSA Collaborative Innovation Center, Shanghai Jiao Tong University, Shanghai 200240, China
(Received 5 May 2017; published 18 December 2017)

A novel scheme for generating a pair of gigawatt attosecond pulses by coherent Thomson scattering from relativistic electron sheets is proposed. With a circularly polarized relativistic laser pulse, the scattered x-ray signal can have a saddlelike temporal profile, where the lower electromagnetic frequencies are found mostly in the center region of this saddlelike profile. By filtering out the latter, we can obtain two few-attosecond pulses separated by a subfemtosecond interval, which is tunable by controlling the energy of the sheet electrons. Such a pulse pair can be useful for an attosecond pump probe at an unprecedented time resolution and for ultrafast chiral studies in molecules and materials.

DOI: 10.1103/PhysRevLett.119.254801

The advent of attosecond light sources has opened the new research area of attosecond science [1–6], which concerns the ultrafast electron dynamics in atoms, molecules, and solids. The attosecond dynamics can be inferred by streaking the attosecond-pulse-released photoelectrons in a background laser field [7,8]. A more direct approach is provided by the use of an attosecond pump probe [9,10]. The pump-probe strategy involves first triggering a system by a pump pulse and then observing the dynamic evolution via a time-delayed probe pulse. Measuring photoelectron spectra as a function of the pulse delay allows one to trace ultrafast processes in the system. Accordingly, an attosecond pump probe requires one pair of temporally synchronized attosecond pulses.

Attosecond-pulse pairs (APPs) are usually produced by high-harmonic generation (HHG) in laser-gas interactions [11–15]. They are typically in the extreme ultraviolet wavelength regime and of hundreds-attosecond duration. They are of nanojoule energy, so that the corresponding power is limited to the megawatt level. The atomic electron dynamics is usually characterized by the atomic time unit $t_{\mathrm{au}} = 24$ as. A snapshot of the atomic electron motion would then require a source of tens of attoseconds or even shorter. Moreover, efficient electron excitation often requires a sufficiently high power source [16]. Some applications, such as studies of inner-shell electron transitions, also demand high photon energies at the 1 keV level [17,18]. These requirements are critical for exploiting the full potential of the attosecond pump-probe technique. However, these requirements are very difficult to achieve by means of the conventional HHG. Free-electron lasers can generate two gigawatt x-ray pulses at 300 eV to 10 keV [19–22], but their duration is on the order of femtoseconds.

Coherent Thomson scattering (CTS) of intense lasers from relativistic electron sheets [23–25] is a promising method for producing gigawatt attosecond pulses near 1 keV. The electron sheets are formed by laser-blown electrons from nanofoils [26,27] or laser-driven plasma waves in underdense plasmas [28–31]. The sheets are only a few nanometers thick but of overcritical density. Electrons in the sheets have a typical energy of tens of MeV with a very narrow (~0.1%) energy spread. The electron energy can be controlled by changing the foil spacing in the laser-driven double-foil scheme [24] or the background plasma density in the laser wakefield scheme [31], respectively. When laser pulses collide head on with the electron sheets, backscattered lights are blueshifted by a Doppler factor of $4\gamma^2$, where γ is the relativistic factor of the sheet. Thus, x rays of 1 keV can be produced with a sheet electron energy of approximately 20 MeV, much lower than that of the electron drivers in free-electron lasers. By a compression ratio of $1/4\gamma^2$, the scattered pulse can easily reach tens of attoseconds. We note that intense attosecond pulses can also be produced by coherent scattering from laser-irradiated nanofilms [32] and solid surfaces [33–35]. Recently, Kiefer *et al.* [36] performed the first experiments on CTS from electron sheets by laser-driven nanofoils and have observed coherent XUV signals.

In this Letter, we report that, for circularly polarized lasers, CTS in a wide nonlinear regime can directly lead to an APP with a tunable subfemtosecond interval. If the laser intensity is beyond a certain threshold, the scattered signal has a saddlelike profile with two peaks in the temporal domain. The peaks are of a higher frequency than the valley between them. This feature can be attributed to the laser amplitude dependence of CTS. Using a proper high-pass filter, we obtain two discrete few-attosecond x-ray pulses. The generation mechanism and interval tuning of APPs are theoretically analyzed and are verified by particle-in-cell (PIC) simulations with the JPIC code [37]. The APPs retain the laser's circular polarization and can be applied to XUV or x-ray magnetic circular dichroism and photoelectron circular dichroism [38,39].

We now discuss the generation process of the APP using a circularly polarized laser pulse. The normalized vector potential of the latter is $\mathbf{a}(\zeta) = a_0 \sin^2(\pi\zeta/T)[\hat{y}\cos(\omega_0\zeta) + \hat{z}\sin(\omega_0\zeta)]$, where $a_0 = eE_0/mc\omega_0$, $\zeta = t + x/c$, T is the pulse

duration, E_0 is the maximum electric field, $\omega_0 = 2\pi/\tau_0$, and $\tau_0 = \lambda_0/c$ is the light cycle. Here e and m are the charge and the mass of an electron, respectively, and c is the speed of light. The electron sheets are assumed to have the density profile $n_e = n_0 \exp[-\pi(x/d_0)^2]$, where n_0 and d_0 are the peak density and characteristic thickness, respectively. The electron sheet in the y, z plane moves along the x axis with the relativistic factor $\gamma_0 = 1/\sqrt{1-\beta_0^2}$, where $\beta_0 = V_0/c$. The nonlinear Doppler factor is given by

$$D(\zeta) = \frac{4\gamma_0^2}{1 + a^2(\zeta)}, \tag{1}$$

so that the CTS signal has the frequency $\omega_s(\zeta) = D(\zeta)\omega_0$. The electric-field amplitude (normalized by $mc\omega_0/e$) of the signal is [25]

$$a_s(\zeta) = \frac{a(\zeta)}{1 + a^2(\zeta)} \frac{\gamma_0 k_0 d_0}{n_c/n_0} e^{-4\gamma_0^4 k_0^2 d_0^2/\{\pi[1+a^2(\zeta)]^2\}}, \tag{2}$$

where k_0 is the wave number and n_c is the critical density. Equations (1) and (2) are valid for multicycle laser pulses with slowly evolving envelopes [40]. The nonlinear term $1 + a^2(\zeta)$ in Eqs. (1) and (2) shows that the scattering process depends on the local laser intensity. That is, the local frequency and amplitude of the scattering signal are generally nonuniform for relativistic laser pulses with $a_0 > 1$.

The scheme for the generation of APPs is demonstrated in Fig. 1, which shows plots of Eqs. (1) and (2). The parameters of the laser are $a_0 = 5$, $T = 10\tau_0$, and $\lambda_0 = 800$ nm, and those of the electron sheet are $\gamma_0 = 20$, $n_0 = 10n_c$, and $d_0 = 0.6$ nm. We see that the scattering frequency is lowest $\omega_{s,0} = 4\gamma_0^2\omega_0/(1 + a_0^2)$ at the laser pulse center, and it approaches the linear limit $4\gamma_0^2\omega_0$ at the laser front and tail. It is striking that two symmetric peaks appear in the scattering amplitude (solid curve), where the scattering efficiency is maximum. This can be attributed to the nonlinear term $1 + a(\zeta)^2$ in Eq. (2). For laser fields with $a \gg 1$, we have the scattering amplitude $a_s \propto 1/a$. These two peaks occur at the certain laser amplitude $a_p = a(\zeta_{1,2})$ in the rising and descending slopes of the laser pulse. It is clear that

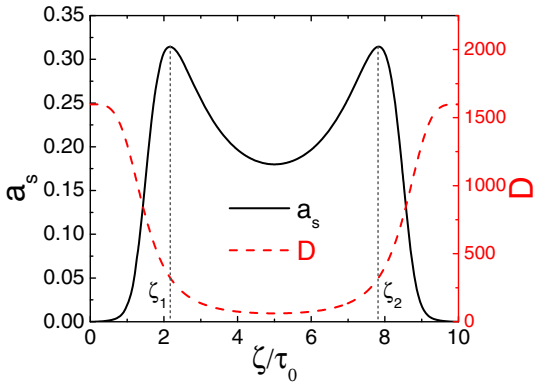

FIG. 1. Scattering amplitude $a_s(\zeta)$ (solid curve) and Doppler factor $D(\zeta)$ (dashed curve) within a laser pulse of $T = 10\tau_0$.

$a_0 > a_p$ is the prerequisite for producing two scattering peaks. By the use of $da_s/da|_{a=a_p} = 0$, we obtain $a_p \approx 2.0$ for the case in Fig. 1. When $a_0 < a_p$, only one peak is produced and the scattered pulse is an isolated attosecond pulse. Note that Eq. (2) is valid only for circularly polarized lasers. PIC simulations show that a linearly polarized laser pulse leads to a train of attosecond pulses due to the $2\omega_0$ beating in the term $a^2(\zeta)$.

Along the cruising direction of the sheet, the scattered light will be compressed in the time domain by the local Doppler factor D. This will result in a saddle-shaped x-ray signal. By sending the signal through a high-pass filter, one can block the middle section (lower frequency and intensity) of the signal and obtain two attosecond pulses. This APP has the frequency $\omega_{s,p} = 4\gamma_0^2\omega_0/(1 + a_p^2)$. We define the frequency contrast of the saddle-shaped signal as

$$\eta = \frac{\omega_{s,p}}{\omega_{s,0}} = \frac{1 + a_0^2}{1 + a_p^2}. \tag{3}$$

In order to realize two discrete pulses, the ratio η should not be close to unity. In Fig. 1, we have $\eta = 5.2$.

To verify the proposed scheme, we have carried out a 1D PIC simulation for the same parameters given in Fig. 1. As displayed in Fig. 2(a), the scattering signal is strongly chirped with a longer wavelength in the middle compared to two peaks. After filtering out the low-frequency components below $4\omega_{s,0}$, we obtain a circularly polarized APP shown in Fig. 2(b). The pulse pair has a photon energy of 398 eV and a pulse interval of 170 as. Each pulse has an intensity FWHM of approximately only 4.5 as. The peak amplitude of the pulse pair from Eq. (2) is 0.31, in agreement with the PIC result.

The pulse interval can be analyzed as follows. During the scattering process, the sheet moves with the longitudinal velocity

$$\beta_x(\zeta) = \frac{4\gamma_0^2 - 1 - a^2(\zeta)}{4\gamma_0^2 + 1 + a^2(\zeta)}, \tag{4}$$

while the laser pulse propagates at the speed of light c in the opposite direction. In the laser pulse, the period for the sheet to move from $\zeta = 0$ to ζ is $t(\zeta) = \int_0^\zeta d\zeta'/[1+\beta_x(\zeta')]$. Meanwhile, the sheet has actually traveled a distance $x(\zeta) = c\int_0^\zeta d\zeta'\beta_x(\zeta')/[1 + \beta_x(\zeta')]$. Then, the scattering signal has the propagation coordinate

$$\begin{aligned}\rho_s(\zeta) &= t(\zeta) - \frac{x(\zeta)}{c} \\ &= \frac{1}{4\gamma_0^2}\left[\zeta + \frac{3a_0^2}{8}\zeta - \frac{a_0^2 T}{4\pi}\sin\left(\frac{2\pi\zeta}{T}\right)\right. \\ &\quad \left. + \frac{a_0^2 T}{32\pi}\sin\left(\frac{4\pi\zeta}{T}\right)\right].\end{aligned} \tag{5}$$

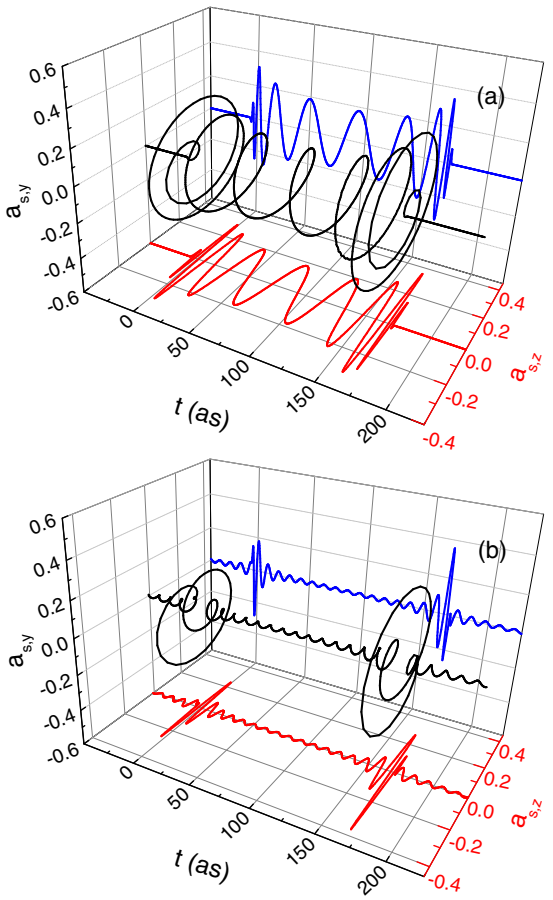

FIG. 2. (a) Electric field a_s of the scattering signal by 1D PIC simulation. (b) APP obtained from (a) after a high-pass filter. Parameters are the same as in Fig. 1.

Two attosecond peaks appear at $a(\zeta_{1,2}) = a_p$, which yields $\zeta_1 = (T/\pi)\arcsin(\sqrt{a_p/a_0})$ and $\zeta_2 = T - \zeta_1$. Finally, we can evaluate the pulse interval by

$$t_d = \rho_s(\zeta_2) - \rho_s(\zeta_1). \tag{6}$$

We obtain $\zeta_1 = 2.2$ and $\zeta_2 = 7.8$ for the case in Fig. 1. Equation (6) gives $t_d = 160$ as, which agrees with the PIC result.

Now we discuss the tunability of the pulse interval. Figure 3(a) displays β_x and ρ_s of the case in Fig. 1. Since laser intensities are low at the laser front and tail, the factor ρ_s remains almost unchanged for $\zeta \le \zeta_1$ and $\zeta \ge \zeta_2$. Accordingly, we can make the approximations $\rho_s(\zeta_1) \approx \rho_s(0)$ and $\rho_s(\zeta_2) \approx \rho_s(T)$. Equation (6) can then be simplified to

$$t_d \approx \left(1 + \frac{3a_0^2}{8}\right)\frac{T}{4\gamma_0^2}, \tag{7}$$

which suggests that varying the electron energy or laser duration can efficiently change the pulse interval.

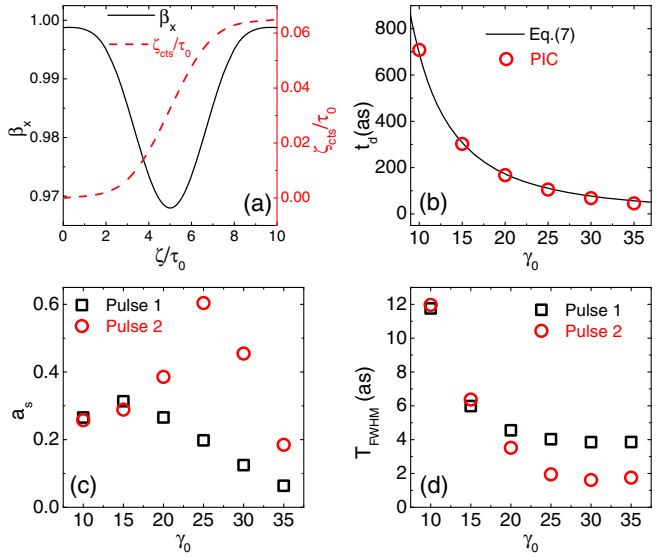

FIG. 3. (a) Electron velocity β_x (solid curve) and signal propagation coordinate ρ_s (dashed curve) for the case in Fig. 1. (b) APP interval, (c) amplitude, and (d) duration versus electron energy γ_0, where the other parameters are the same as in Fig. 2.

Figure 3(b) shows that the pulse interval t_d is flexibly tunable within one femtosecond by adjusting γ_0 for the fixed laser parameters. The PIC results are well reproduced by Eq. (7). As displayed in Figs. 3(c) and 3(d), the APP amplitude and duration also change with the electron energy. Equation (2) predicts that the amplitude of the two peaks shall gently increase with the electron energy. Nevertheless, we note that the first pulse weakens for $\gamma_0 \ge 15$ and the second pulse is the strongest at $\gamma_0 = 25$. As a whole, one can see that the second pulse is more intense than the first one. PIC simulations show that the electron sheets get compressed longitudinally during the CTS, and their increased densities boost the second pulse. For the case of $\gamma_0 = 25$, the sheet shortens to about a quarter of the original thickness when producing the second pulse. This drift compression should be mainly caused by the different electron velocities in the sheet at the front of the laser pulse given by Eq. (4). Finally, the pulse duration monotonically decreases with the electron energy. The APP amplitude and duration are also affected by the cutoff frequency of the filter.

Two-dimensional PIC simulations have been done to study multidimensional effects on the APP production. The simulation box is $14\lambda_0 \times 10\lambda_0$ in the x, y plane, and the cell size is $(\lambda_0/5000) \times (\lambda_0/128)$. The laser pulse has a spot size $\sigma = 10\lambda_0$. The sheet electrons are distributed in $2.5\lambda_0 < y < 7.5\lambda_0$, uniformly in the y direction with $n_0 = 6n_c$. The other parameters and interaction geometry are the same as in the 1D PIC simulation in Fig. 2. Figure 4(a) shows the s-polarized component $a_{s,z}$ (along the z direction) of the circularly polarized scattering signal. Interestingly, the signal has a curved-focusing phase front at the tail, in accordance with the deformed sheet shown in

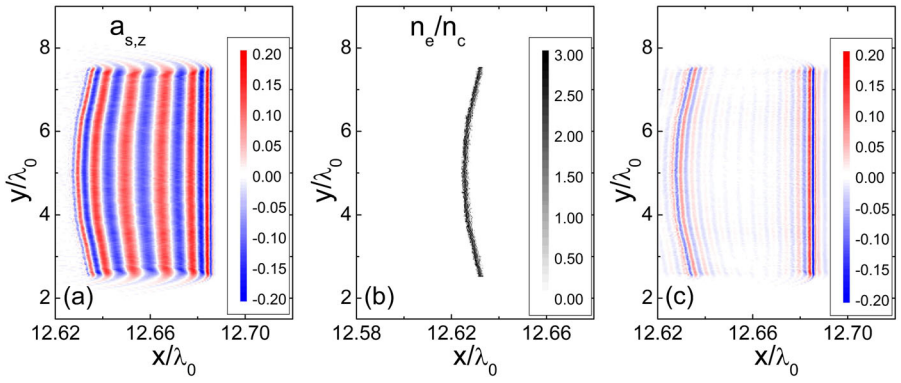

FIG. 4. (a) Electric field $a_{s,z}$ of the scattering signal from the 2D PIC simulation. (b) Electron density n_e/n_c of the sheet at the same moment as (a). (c) APP obtained from (a) by a high-pass filter.

Fig. 4(b). The longitudinal deformation of the sheet is $\triangle x \approx 6 \times 10^{-3}\lambda_0$. The sheet is deformed, because the electron longitudinal velocity β_x [Eq. (4)] depends on the Gaussian laser amplitude with $a(y) \propto \exp(-y^2/\sigma^2)$, and electrons on the laser axis have a smaller velocity than off-axis ones. After filtering out the low-frequency components below $3\omega_{s,0}$, two pulses of the obtained APP in Fig. 4(c) have intensities of 9.5×10^{16} and 1.7×10^{16} W/cm^2 and durations of 5 and 10 as. The second pulse is weaker because of the reduction of the sheet density by Coulomb expansion. For the source size of about $5\lambda_0$, these two attosecond pulses have 12 and 2 GW in peak power, respectively.

Two attosecond pulses from the HHG are produced by impinging a laser pulse on one [14,15] or two successive [11,13] gas jets. The single laser drive ensures the synchronization and collinearity of the APP. The present scheme possesses these merits as well. Importantly, since both attosecond pulses are radiated from the single nanosheet, they are also correlated in their absolute phases, as shown in Figs. 2 and 4. The relativistic Doppler effect allows the efficient compression of the pulse duration down to ~5 as, much shorter than the atomic time unit t_{au}. Moreover, since it is free from material breakdown as in HHG, the APPs from coherent laser-electron scattering can be 3–4 orders of magnitude more powerful than the HHG sources.

In conclusion, we have presented a robust method for obtaining a pair of attosecond pulses. The method is based on the nonlinear interaction between relativistic electron sheets and femtosecond circularly polarized lasers of relativistic intensity. The resulting APPs have a duration of sub-10-as each, and their interval is adjustable within one femtosecond. This new type of APP can push the attosecond pump-probe system to an unprecedented time resolution. It can be utilized to film the electron motion in atoms, such as the details of tunneling ionization [41,42]. Meanwhile, its circular polarization allows one to diagnose the chiral and magnetic properties in materials.

This work was supported by the Thousand Youth Talents Plan, National Natural Science Foundation of China (No. 11374262 and No. 1627901), and Fundamental Research Funds for the Central Universities. The authors thank M. Y. Yu for helpful comments.

*huichunwu@zju.edu.cn

[1] F. Krausz and M. Ivanov, Rev. Mod. Phys. **81**, 163 (2009).
[2] P. Agostini and L. F. DiMauro, Rep. Prog. Phys. **67**, 813 (2004).
[3] A. Scrinzi, M. Yu. Ivanov, R. Kienberger, and D. M. Villeneuve, J. Phys. B **39**, R1 (2006).
[4] P. H. Bucksbaum, Science **317**, 766 (2007).
[5] M. Nisoli and G. Sansone, Prog. Quantum Electron. **33**, 17 (2009).
[6] M. Schultze *et al.*, J. Electron Spectrosc. Relat. Phenom. **184**, 68 (2011).
[7] M. Drescher, M. Hentschel, R. Kienberger, M. Uiberacker, V. Yakovlev, A. Scrinzi, Th. Westerwalbesloh, U. Kleineberg, U. Heinzmann, and F. Krausz, Nature (London) **419**, 803 (2002).
[8] M. Schultze *et al.*, Nature (London) **493**, 75 (2013).
[9] S. X. Hu and L. A. Collins, Phys. Rev. Lett. **96**, 073004 (2006).
[10] J. Mauritsson *et al.*, Phys. Rev. Lett. **105**, 053001 (2010).
[11] E. M. Bothschafter, A. Schiffrin, V. S. Yakovlev, A. M. Azzeer, F. Krausz, R. Ernstorfer, and R. Kienberger, Opt. Express **18**, 9173 (2010).
[12] P. Tzallas, E. Skantzakis, L. A. A. Nikolopoulos, G. D. Tsakiris, and D. Charalambidis, Nat. Phys. **7**, 781 (2011).
[13] D. Fabris, T. Witting, W. A. Okell, D. J. Walke, P. Matia-Hernando, J. Henkel, T. R. Barillot, M. Lein, J. P. Marangos, and J. W. G. Tisch, Nat. Photonics **9**, 383 (2015).
[14] A. Guggenmos, J. Schmidt, S. Heinrich, B. Nickel, F. Krausz, and U. Kleineberg, in *Frontiers in Optics*, OSA Technical Digest (Optical Society of America, Washington, DC, 2015), paper FM3A.3.
[15] F. Campi, H. Coudert-Alteirac, M. Miranda, L. Rading, B. Manschwetus, P. Rudawski, A. L'Huillier, and P. Johnsson, Rev. Sci. Instrum. **87**, 023106 (2016).

[16] F. Lépine, M. Y. Ivanov, and M. J. J. Vrakking, Nat. Photonics **8**, 195 (2014).
[17] N. Rohringer *et al.*, Nature (London) **481**, 488 (2012).
[18] S. M. Vinko *et al.*, Nature (London) **482**, 59 (2012).
[19] A. A. Lutman, R. Coffee, Y. Ding, Z. Huang, J. Krzywinski, T. Maxwell, M. Messerschmidt, and H.-D. Nuhn, Phys. Rev. Lett. **110**, 134801 (2013).
[20] E. Allaria *et al.*, Nat. Commun. **4**, 2476 (2013).
[21] T. Hara *et al.*, Nat. Commun. **4**, 2919 (2013).
[22] A. Marinelli *et al.*, Nat. Commun. **6**, 6369 (2015).
[23] J. Meyer-ter-Vehn and H.-C. Wu, Eur. Phys. J. D **55**, 433 (2009).
[24] H.-C. Wu, J. Meyer-ter-Vehn, J. Fernández, and B. M. Hegelich, Phys. Rev. Lett. **104**, 234801 (2010).
[25] H.-C. Wu, J. Meyer-ter-Vehn, B. M. Hegelich, and J. C. Fernández, Phys. Rev. ST Accel. Beams **14**, 070702 (2011).
[26] V. V. Kulagin, V. A. Cherepenin, M. S. Hur, and H. Suk, Phys. Rev. Lett. **99**, 124801 (2007).
[27] B. Dromey *et al.*, Nat. Phys. **8**, 804 (2012).
[28] S. V. Bulanov, T. Esirkepov, and T. Tajima, Phys. Rev. Lett. **91**, 085001 (2003).
[29] M. Kando *et al.*, Phys. Rev. Lett. **99**, 135001 (2007).
[30] M. Kando *et al.*, Phys. Rev. Lett. **103**, 235003 (2009).
[31] F. Y. Li, Z. M. Sheng, Y. Liu, J. Meyer-ter-Vehn, W. B. Mori, W. Lu, and J. Zhang, Phys. Rev. Lett. **110**, 135002 (2013).
[32] K. Lee, B. H. Kim, and D. Kim, Phys. Plasmas **12**, 043107 (2005).
[33] R. Lichters, J. Meyer-ter-Vehn, and A. Pukhov, Phys. Plasmas **3**, 3425 (1996).
[34] T. Baeva, S. Gordienko, and A. Pukhov, Phys. Rev. E **74**, 065401 (2006).
[35] U. Teubner and P. Gibbon, Rev. Mod. Phys. **81**, 445 (2009).
[36] D. Kiefer *et al.*, Nat. Commun. **4**, 1763 (2013).
[37] H.-C. Wu, arXiv:1104.3163.
[38] D. D. Hickstein *et al.*, Nat. Photonics **9**, 743 (2015).
[39] A. A. Lutman *et al.*, Nat. Photonics **10**, 468 (2016).
[40] K. Hu and H.-C. Wu, Opt. Lett. **41**, 4586 (2016).
[41] D. Shafir, H. Soifer, B. D. Bruner, M. Dagan, Y. Mairesse, S. Patchkovskii, M. Yu. Ivanov, O. Smirnova, and N. Dudovich, Nature (London) **485**, 343 (2012).
[42] O. Pedatzur *et al.*, Nat. Phys. **11**, 815 (2015).